2015 IEEE International Conference on Robotics and Automation (ICRA)
Washington State Convention Center
Seattle, Washington, May 26-30, 2015

Snakeboard Motion Planning with Viscous Friction and Skidding

Tony Dear[1], Scott David Kelly[2], Matthew Travers[1], and Howie Choset[1]

Abstract— **The snakeboard is a well-studied example for mechanical systems analysis, largely because of its simultaneous richness in behavior and simplicity in design. However, few snakeboard models incorporate dissipative friction in the traveling direction and skidding as a violation of the rigid nonholonomic constraints. In this paper we investigate these effects on trajectory planning by evaluating a previously proposed friction model as well as a novel skidding model based on the addition of Rayleigh dissipation functions. We show how these additions change the usual behavior of gaits in the forward planning problem, and incorporate the changes into the solutions of the inverse planning problem by utilizing body coordinates along with a curvature parameterization for trajectories.**

Fig. 1: A snakeboard, composed of a rigid axis and two footrests on rotating wheelsets.

I. Introduction

The snakeboard is a canonical example of a mixed nonholonomic mechanical system, one whose motion is governed by both kinematic constraints and dynamics [1], [2]. The snakeboard shown in Fig. 1 consists of two sets of wheels that can rotate about the center point of the axle. To ride the snakeboard, one alternates between rotating one's torso with one's ankles to move the wheelsets. The mechanical model (Fig. 2) has a rotor situated at the center of the longitudinal axis to simulate the human rider's torso. The rotor and wheel axle angles are actuated, and the latter are nonholonomically constrained, allowing the snakeboard to locomote due to input joint actuation.

Early approaches in snakeboard analysis employed extensive use of gaits, or cyclic changes in the joint inputs. Ostrowski et al. [3] used techniques developed by Murray and Sastry [4] to evaluate sinusoidal steering controllers to move the snakeboard in various basis directions. Ostrowski et al. [5] then extended this approach by using optimal control to select optimal gaits for their controllers.

Bullo and Lewis [6] addressed the motion planning problem of taking a snakeboard to a desired goal state from a start state by using vector field analysis techniques developed by Bullo and Lynch [7]. In these solutions, the snakeboard's overall trajectory was a concatenation of separate kinematic trajectory segments between the start and goal states.

In order to study the contributions of gaits to locomotion, Shammas et al. [2] analyzed gait motions as a combination of geometric and dynamic displacement contributions. They were able to propose gaits that contribute to motion along a desired direction, although their method did not address the full motion planning problem of finding a trajectory between two states in the workspace.

More recently, Shammas and de Oliveira [8], [9] developed a solution for the snakeboard in which the problem specification was an entire workspace trajectory instead of only the endpoint configurations. Their approach removed joint constraints and use of gaits, allowing for an analytical solution for the joint angles in order to follow the prescribed trajectory. This work was then extended by Dear et al. [10], who proposed an alternate representation of the solution using only body coordinates and local curvature information of the desired trajectory. This allowed for simple path primitives that can be stitched together to form more complex trajectories.

Separately from motion planning, the geometric mechanics community has addressed dissipative forces for mechanical systems, often in the form of a Rayleigh dissipation function. Kelly and Murray [11] treated viscous drag as a connection form on a principal fiber bundle, analogous to the mechanical connection due to inertial effects or nonholonomic constraints [12]. Ostrowski [13] computed the reduced equations for nonholonomic systems with dissipative forces and illustrated the results on some simple snakeboard gaits.

On the contrary, the issue of skidding has not found much treatment in geometric and analytic models, and is instead often addressed by sensor measurements and corrective control strategies. Sidek and Sarkar [14] were able to include skidding in a system's dynamic model by relaxing the nonholonomic constraints. Bazzi et al. [15], [16] then extended this work by modifying the model so as to preserve the original constraint form, allowing for the computation of the reduced equations as in previous models.

Thus far, geometric analysis of drag and skid has largely been confined to simple systems like the mobile car and vertical rolling disk, and neither effect has been incorporated into locomotion planning for mixed systems like the snakeboard. In the present paper, we first review the development of the

[1]T. Dear, M. Travers, and H. Choset are with the Robotics Institute at Carnegie Mellon University, Pittsburgh, PA 15213, USA. {tonydear@, mtravers@andrew., choset@cs.}cmu.edu

[2]S. D. Kelly is with the Department of Mechanical Engineering and Engineering Science at the University of North Carolina at Charlotte, Charlotte, NC 28223, USA. scott@kellyfish.com

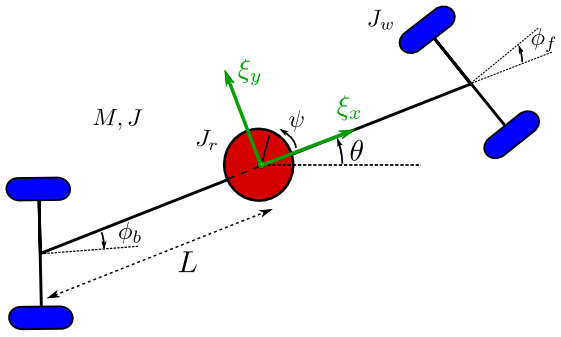

Fig. 2: The configuration of the snakeboard. Parameters include M, L, J, J_r, and J_w. The joint angle inputs are ψ and $\phi = \phi_f = -\phi_b$. We can define a body frame at the rotor, giving us body velocities ξ_x, ξ_y, and ξ_θ.

inverse trajectory planning problem and solution of [10] in Section II. In Section III we compensate for viscous friction by appending the damping model of [13] to our solution; in Section IV, we develop a novel model of skidding. Both models are based on the addition of an appropriate Rayleigh dissipation function, allowing us to turn to established results from geometric mechanics for integration into our model.

II. Snakeboard Locomotion in Body Coordinates

We review the background describing the mechanics of snakeboard locomotion. We emphasize that our approach will primarily rely on the usage of body coordinates, as opposed to world or inertial coordinates. This distinction will be made clear below. For more details on the subject, see [10].

A. Equations of Motion

The snakeboard's configuration, shown in Fig. 2, is given by $q \in Q = (g, r)$, where the position variables $g = (x, y, \theta) \in G = SE(2)$ locate the snakeboard in the world and the shape variables $r = (\psi, \phi) \in M = \mathbb{S}^1 \times \mathbb{S}^1$ describe the joint configurations. The variables x and y denote the global position of the center of mass at the rotor, while θ denotes the system's orientation with respect to the inertial x axis. ψ denotes the rotor angle, and ϕ_f and ϕ_b denote the angles of the front and back wheels, respectively, with respect to the longitudinal axis. We enforce the constraint $\phi_f = -\phi_b$ and henceforth use $\phi = \phi_f$.

The snakeboard's body frame is situated at the rotor, with its velocities ξ representing components in the forward, lateral, and rotation directions. We can relate ξ to the world velocity $\dot{g} = (\dot{x}, \dot{y}, \dot{\theta})$ by the following mapping:

$$\xi = \begin{pmatrix} \xi_x \\ \xi_y \\ \xi_\theta \end{pmatrix} = \begin{pmatrix} \cos\theta & \sin\theta & 0 \\ -\sin\theta & \cos\theta & 0 \\ 0 & 0 & 1 \end{pmatrix} \begin{pmatrix} \dot{x} \\ \dot{y} \\ \dot{\theta} \end{pmatrix}. \quad (1)$$

The snakeboard's mass and inertia are denoted M and J, while the rotor and wheel inertias are denoted J_r and J_w. We assume that $ML^2 = J + J_r + 2J_w$ is the total inertia of the system, where the total length of the snakeboard is $2L$.

The snakeboard's Lagrangian is invariant to changes in the system's position or orientation in space ($SE(2)$) due to symmetry, so we can express it in body velocities instead of world velocities. The Lagrangian in the body frame becomes

$$l(\xi, \dot{r}) = \frac{1}{2}M(\xi_x^2 + \xi_y^2 + L^2\xi_\theta^2) + \frac{1}{2}J_r\dot{\psi}^2 + J_r\xi_\theta\dot{\psi} + J_w\dot{\phi}^2. \quad (2)$$

Standard models assume no-slip nonholonomic constraints on the wheelsets. Like the Lagrangian, the constraints are invariant with respect to transformations in $SE(2)$, so they can be written in terms of the local body coordinates only. They can be expressed in *Pfaffian form* $\omega(r)\xi = 0$, where

$$\omega(r) = \begin{pmatrix} \omega_f \\ \omega_b \end{pmatrix} = \begin{pmatrix} -\sin\phi & \cos\phi & L\cos\phi \\ \sin\phi & \cos\phi & -L\cos\phi \end{pmatrix}. \quad (3)$$

Instead of writing out the full Euler-Lagrange equations of motion, we take advantage of the nonholonomic constraints to derive the reduced equations of motion. From (2) and (3) we first compute the *nonholonomic momentum* [12] using the definition $p_{\text{nh}} = \langle \frac{\partial l}{\partial \xi}; \Omega \rangle$, where Ω is a basis of the null space of ω. We choose $\Omega = (L, 0, \tan\phi)^T$ and find

$$p_{\text{nh}} = ML(\xi_x + L\xi_\theta \tan\phi) + J_r\dot{\psi}\tan\phi. \quad (4)$$

Next we examine how joint velocities and momentum determine resultant body velocities. Combining the constraints (3) and the momentum definition (4), we find the following *reconstruction equation*.

$$\xi = -\begin{pmatrix} \frac{J_r \sin 2\phi}{2ML} & 0 \\ 0 & 0 \\ \frac{J_r \sin^2\phi}{ML^2} & 0 \end{pmatrix} \begin{pmatrix} \dot{\psi} \\ \dot{\phi} \end{pmatrix} + \begin{pmatrix} \frac{\cos^2\phi}{ML} \\ 0 \\ \frac{\sin 2\phi}{2ML^2} \end{pmatrix} p_{\text{nh}} \quad (5)$$

Finally, we solve for the *momentum evolution equation* [12], which describes how the momentum changes in time. Referencing the formulation in [13], we have

$$\dot{p}_{\text{nh}} = \left\langle \frac{\partial l}{\partial \xi}; [\xi, \Omega] + \dot{\Omega} \right\rangle = \dot{\phi}\sec^2\phi(ML^2\xi_\theta + J_r\dot{\psi}), \quad (6)$$

where $[\cdot, \cdot]$ denotes the Lie bracket operation. If we substitute in the constraint equations $\omega(r)\xi = 0$, we can eliminate the body velocities and obtain a differential equation in p_{nh}.

$$\dot{p}_{\text{nh}} = \dot{\phi}(p_{\text{nh}}\tan\phi + J_r\dot{\psi}) \quad (7)$$

Equations (5) and (7) constitute the first-order equations of motion for the snakeboard. Given shape inputs ϕ, ψ, and their derivatives, we can completely determine the snakeboard's configuration velocities. In particular, [3], [5] developed periodic inputs, or gaits, to achieve motion primitives such as forward movement, rotation, and parallel parking.

B. Motion Planning

Given a desired trajectory in space, the motion planning problem is to determine the joint inputs that will allow the snakeboard's COM to track it. A trajectory in $SE(2)$ is often described in inertial coordinates as functions of time; by the fundamental theorem of curves [17], one can equivalently use an arclength and curvature parameterization. Let $r(t)$ denote the distance along the path, at time t, from the path starting point; for example, if t_0 is the starting time, then $r(t_0)$ is necessarily equal to 0. Let $\kappa(r)$ denote the curvature along

the path. We can then define $c(t) := \kappa(r(t))$ to be the path curvature as a function of time. For example, $c(t_0) = \kappa(0)$ is the curvature of the path starting point.

As in [9] and [10], we also require ξ_x to be instantaneously tangent to the path while the COM tracking it, as shown in Fig. 3. If the local curvature at the point of contact is κ, then $R = |\kappa^{-1}|$ is the radius of curvature from the instantaneous center of rotation O. The snakeboard can then be represented by a generalized bicycle model [18], which requires that the wheelsets' disallowed directions of motion meet at O. This provides us a simple geometric solution for the wheel angle input in terms of the known path curvature function.

$$\phi(t) = \tan^{-1}(Lc(t)) \tag{8}$$

We can now establish a relationship between the body velocities and the trajectory profile. First we note that imposing the body tangency requirement enforces that $\xi_x(t)$, the forward velocity of the snakeboard, be exactly equal to $\dot{r}(t)$, the magnitude of the velocity vector along the trajectory. Combining this with the constraints (3), we have that

$$\xi(t) = \begin{pmatrix} \xi_x(t) \\ \xi_y(t) \\ \xi_\theta(t) \end{pmatrix} = \begin{pmatrix} \dot{r}(t) \\ 0 \\ c(t)\dot{r}(t) \end{pmatrix}. \tag{9}$$

In the last step, we solve for the rotor input profile, $\dot{\psi}(t)$. If we differentiate the momentum in (4) and equate it to (7), we can eliminate p_{nh} and obtain an equation in the body velocities and shape variables. Replacing the body velocities with trajectory information using (9), we can obtain a solution for $\ddot{\psi}(t)$ (and via integration, $\dot{\psi}(t)$).

$$\ddot{\psi}(t) = -\frac{M}{J_r}\left(\frac{1}{c(t)} + L^2 c(t)\right)\ddot{r}(t) - \frac{ML^2}{J_r}\dot{c}(t)\dot{r}(t) \tag{10}$$

Given (8) and (10), the joint inputs can be numerically determined from the curvature and velocity profile of the desired trajectory. Certain trajectories may yield analytical solutions for $\dot{\psi}$ by explicit integration of (10). Dear et al. [10] goes over these special trajectories in more detail, along with cases of zero and infinite curvature; it is shown that we lose controllability in the former case, whereas the latter can be dealt with using angular momentum conservation.

III. Viscous Friction in Travel Direction

We now consider friction acting on the wheels in the direction of travel. Ostrowski [13] represented these forces by a group-invariant Rayleigh dissipation function, deriving the new reduced equations and illustrating the results on the snakeboard's forward equations. We first briefly review these results and then incorporate them into the inverse planning solutions for ϕ and $\ddot{\psi}$.

A. Motion Planning Solution

In order to define the dissipation function, we require the velocities at the center of each wheelset. Analogous to constraint directions $\omega(r)$ in (3), we can write down similar equations for the reduced forward velocities of the wheelsets:

$$\begin{pmatrix} v_f \\ v_b \end{pmatrix} = \begin{pmatrix} \cos\phi & \sin\phi & L\sin\phi \\ \cos\phi & -\sin\phi & L\sin\phi \end{pmatrix} \xi, \tag{11}$$

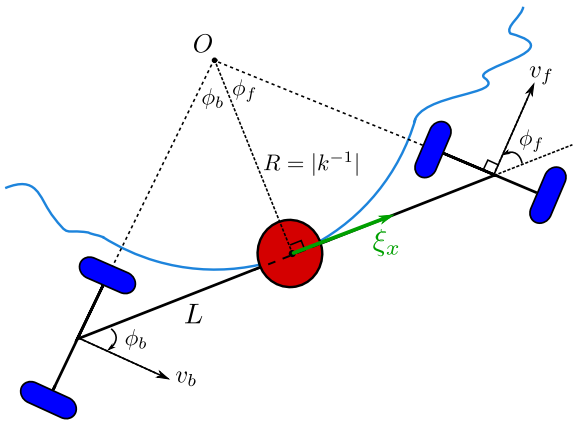

Fig. 3: The geometry of the snakeboard's trajectory. The COM's velocity is instantaneously tangent to a path with curvature κ. This allows us to define a circle with radius R, with the wheelset axes intersecting at the circle center O.

where v_f and v_b are the instantaneous velocity components of the front and back wheelsets, respectively (see Fig. 3).

We assume the same damping coefficient, k_d, for both wheelsets. Because the velocities in (11) are group-invariant, we can write a reduced *damping* Rayleigh dissipation function, proportional to the squares of the velocities.

$$R_{\text{damp}}(r, \xi) = \frac{1}{2}k_d(v_f^2 + v_b^2) \tag{12}$$

The inclusion of this dissipation function leaves our derivations unchanged up to the the momentum evolution equation (6). As shown by [13], the time change in momentum now takes on an additional term to account for the damping in the valid travel directions.

$$\dot{p}_{\text{damp}} = \left\langle \frac{\partial l}{\partial \xi}; [\xi, \Omega] + \dot{\Omega} \right\rangle - \left\langle \frac{\partial R_{\text{damp}}}{\partial \xi}; \Omega \right\rangle \tag{13}$$

The expression for p_{damp} is the same as that for p_{nh}; we introduce the new variable as its evolution equation (13) is different. Specifically, we can compute the new term by using the same Ω as before, and add the result to (7) to obtain

$$\dot{p}_{\text{damp}} = \dot{\phi}(p_{\text{damp}}\tan\phi + J_r\dot{\psi}) - \frac{2k_d}{M}(p_{\text{damp}} - J_r\dot{\psi}\tan\phi). \tag{14}$$

Note the change in behavior induced by the damping terms. As expected, there is a retarding force on the system proportional to its current momentum p_{damp}. If we lock the wheelsets while locomoting ($\dot{\phi} = 0$), then p_{damp} exponentially approaches an equilibrium determined by $\dot{\psi}$. Ostrowski [13] showed the effect of a range of damping coefficients on various snakeboard gaits.

Our contribution is to incorporate the new damping terms into our joint solutions for the motion planning problem. Note that the wheel angle solution (8) does not change, as it is solely a function of trajectory curvature. On the other hand, if we follow the same process in solving for the rotor profile

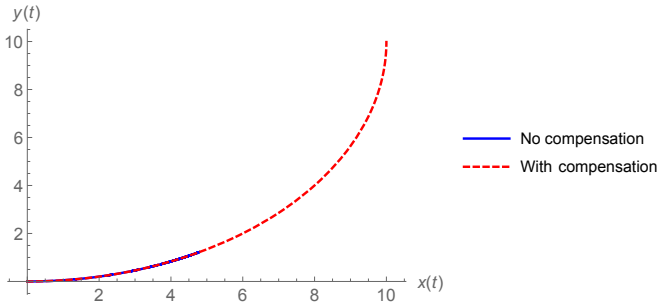

Fig. 4: Comparison of resultant trajectories due to controllers without and with damping compensation. The latter is able to travel the required distance while the former lags far behind.

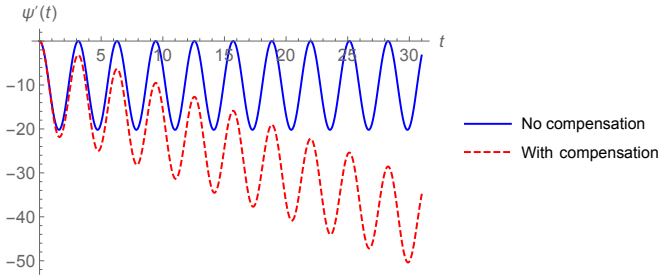

Fig. 5: Rotor velocity comparison for scenario in Fig. 4. While the latter controller is superior for trajectory tracking, it causes the rotor velocity to grow unbounded.

by differentiating (4) and equating it to (14), we obtain

$$\ddot{\psi}_{\text{damp}}(t) = \ddot{\psi}(t) - \frac{2k_d}{J_r}\left(\frac{1}{c(t)} + L^2 c(t)\right)\dot{r}(t). \qquad (15)$$

B. Discussion and Simulations

The new solution (15) allows us to determine the required rotor input given a trajectory to track. Unlike in [10], we cannot find $\dot{\psi}(t)$ explicitly for general trajectories with constant velocity but varying curvature, due to integral dependence on $c(t)$. If instead we consider constant nonzero curvature c_0, we can obtain an analytical solution in the form

$$\begin{aligned}\dot{\psi}_{\text{cc}}(t) = &-\frac{M}{J_r}\left(\frac{1}{c_0} + L^2 c_0\right)(\dot{r}(t) - \dot{r}(t_0)) \qquad (16)\\ &-\frac{2k_d}{J_r}\left(\frac{1}{c_0} + L^2 c_0\right)(r(t) - r(t_0)) + \dot{\psi}(t_0),\end{aligned}$$

where t_0 is the time at which $c(t)$ becomes constant.

Consider an example of a constant curvature trajectory with curvature function $c(t) = 0.1$ and a velocity profile $\dot{r}(t) = \sin^2(t)$. Here the snakeboard executes a periodic stop-and-go trajectory around a circle of radius 10. Along with the initial conditions $(x(0), y(0), \theta(0)) = (0, 0, 0)$, we use the following parameters, which will be the same in all simulations that follow.

$$M = 4, \quad J_r = 2, \quad J_w = 0.5, \quad J = 1, \quad L = 1$$

Fig. 4 simulates the snakeboard's motion in the case of damping coefficient $k_d = 0.2$ for the two controllers (10) and (16) for about 31 seconds. Integrating our velocity function $\dot{r}(t)$ and evaluating the result at $t = 31$, we expect the system to have traveled a distance of about 15.7, or a quarter of the circle. This is exactly what we get with the damping-compensated controller (16), while the other is greatly slowed down by damping.

However, we note that for practical purposes the controller (16) may be difficult to implement. As shown in Fig. 5, the rotor velocity actually grows unbounded, while the original controller does not lead to this effect. This is expected because the amount of damping compensation, which leads to a slightly greater rotor velocity each cycle, is cumulative as the snakeboard travels more distance.

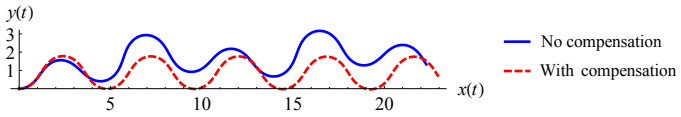

Fig. 6: Serpenoid trajectory comparison for controllers without and with damping compensation. The latter controller for $\dot{\psi}$ saturates near small curvatures, but it is still able to track the desired path much more closely than the former.

The problem of unbounded rotor velocity can be addressed by utilizing a rotor "reset." To perform this maneuver, the snakeboard must be allowed to stop for a finite amount of time; hence $\dot{r}(t) = \sin^2(t)$ cannot be followed exactly. Once the system is stopped, we rotate its wheel angles to $\phi = 0$, rendering the snakeboard uncontrollable. Because it cannot locomote in this state, we can then reset its rotor velocity to 0, and then unrotate the wheel angles and resume as before. For further details on this technique, see [10].

For solutions of the general controller (15), this reset manuever may be particularly useful for nearly straight trajectories or dealing with corners or kinks in the path. As either $c \to 0$ or $c \to \infty$, $\dot{r}$ would have to decrease appropriately; in the limit, we have that a feasible $\dot{r}$ must be 0 and the snakeboard stops moving for both cases.

However, we can observe that if the system reaches these difficult conditions only momentarily, then (15) can still perform adequate tracking without deviating from the trajectory to reset. We consider the serpenoid curve [19], which is characterized by a curvature function of the form $c(t) = a\cos(bt)$, where a and b are parameters. Here we take $a = b = 1$ and prescribe constant unit speed ($\dot{r} = 1$). On this trajectory, the curvature periodically decreases to 0.

Fig. 6 compares the snakeboard's motion for the controllers (10) and (15), again with $k_d = 0.2$. For the latter, we clip the velocity where it becomes large (the clipping value is the maximum velocity from the solution of (10)). It is clear that even with the imposed saturation on the rotor, (15) produces a serpenoid trajectory much closer to the friction-free case than that due to (10).

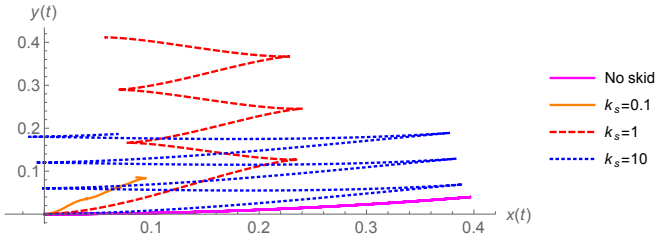

Fig. 7: Resultant trajectories from constant curvature joint inputs over a range of skidding constants. The path degrades more and more from the ideal, no-skid case as k_s decreases.

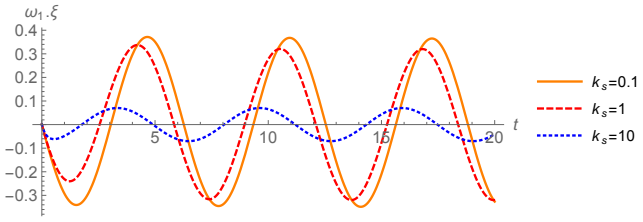

Fig. 8: Front wheel velocities orthogonal to direction of travel (skidding velocities) for the trajectories in Fig. 7. The skidding components become larger as k_s decreases.

IV. Skidding Orthogonal to Travel Direction

If the snakeboard's wheels skid, then the nonholonomic constraints are violated, as the wheel velocities have components in the no-travel directions. However, moving orthogonal to the directions of the wheelsets should still generate large resistive forces. We therefore propose to replace the "hard" nonholonomic constraints with "soft" dissipative forces, modeled by a *skidding* Rayleigh dissipation function.

$$R_{\text{skid}}(r,\xi) = \frac{1}{2}k_s\left((\omega_f\xi)^2 + (\omega_b\xi)^2\right) \tag{17}$$

Here, k_s is a skidding coefficient, and the vectors ω_f and ω_b are the same as those in (3). These directions are orthogonal to the ones used in the damping dissipation function (12).

A. Equations of Motion

To compute the equations of motion, we can evaluate the reduced Euler-Lagrange equations augmented with the dissipative forces from the Rayleigh dissipation function.

$$\frac{d}{dt}\left(\frac{\partial l(r,\xi)}{\partial \xi_i}\right) = -\frac{\partial R_{\text{skid}}(r,\xi)}{\partial \xi_i}; \quad i = x, y, \theta \tag{18}$$

Note that the partial derivatives of the Lagrangian with respect to the position variables vanish from the equations, as the Lagrangian is cyclic in those variables.

We can also reformulate the equations (18) in the form of a reconstruction equation together with a momentum evolution equation, analogous to (5) and (6). Referencing [11], [20] for the inclusion of dissipation in this form, we have

$$\xi = -\begin{pmatrix} 0 & 0 \\ 0 & 0 \\ \frac{J_r}{ML^2} & 0 \end{pmatrix}\begin{pmatrix}\dot{\psi}\\ \dot{\phi}\end{pmatrix} + \begin{pmatrix} \frac{1}{M} & 0 & 0 \\ 0 & \frac{1}{M} & 0 \\ 0 & 0 & \frac{1}{ML^2}\end{pmatrix} p \tag{19}$$

$$\dot{p} = \begin{pmatrix} -2k_s\sin^2(\phi) & 0 & k_sL\sin(2\phi) \\ 0 & -2k_s\cos(\phi) & 0 \\ k_sL\sin(2\phi) & 0 & -2k_sL^2\cos^2(\phi)\end{pmatrix}\xi,$$

where $p = \frac{\partial l}{\partial \xi}$ is the *generalized momentum*. Unlike the nonholonomic momentum p_{nh}, there are three momenta components since there are no longer any hard constraints restricting the system's motion. From the above equations, we see that as $k_s \to 0$, it becomes harder to change p and subsequently ξ_x and ξ_y. Indeed, in the absence of friction entirely, applying a rotor input $\dot{\psi}$ will only affect angular velocity due to conservation of angular momentum.

To evaluate our model, we look at the behavior of the snakeboard over a range of skidding coefficients k_s. Consider the following shape inputs describing an oscillation along a constant curvature path, $\dot{\psi}(t) = -\sin(t)$ and $c(t) = 0.5$. With the regular nonholonomic constraints in place, the snakeboard oscillates along the same curve without going off its path, shown in Fig. 7. But if the system is allowed to skid, it deviates from its path and continues to do so as the gait is executed. Interestingly, the resultant trajectories are reminiscent of the "parallel parking" gait described in [13].

A second observation for this example is that the path deviations are more pronounced for small k_s; as k_s increases, the resultant trajectory becomes closer to the ideal one. We can also see this effect in Fig. 8, which shows the velocity component of the front wheel in the skidding (perpendicular to travel) direction, denoted by $\omega_f\xi$. This quantity is 0 for the no-skid case, and becomes larger as k_s decreases. Finally, we note that while the skidding velocities for the $k_s = 0.1$ and $k_s = 1$ cases are qualitatively similar, the corresponding trajectories in Fig. 7 are still very different, as the snakeboard is spinning more than translating in the former case.

B. Motion Planning Solution

Given our new model of system behavior, we would still like to derive explicit controllers for the shape inputs to track a given trajectory. A first approach would be to reuse the body velocity relationships with the desired trajectory (9). If we substitute these equations into (18), we can then numerically solve for inputs that move the system around *as if the constraints were in place*.

$$\begin{aligned} 0 &= -M\ddot{r} + k_s(L\sin(2\phi)c - 2\sin^2(\phi))\dot{r} \\ J_r\ddot{\psi} &= -ML^2(c\ddot{r} + \dot{c}\dot{r}) + k_sL(\sin(2\phi) - 2L\cos^2(\phi)c)\dot{r} \end{aligned} \tag{20}$$

Given that we know the parameterization of the desired trajectory in $r(t)$ and $c(t)$, we can solve the first line of (20) for ϕ, followed by the solution for $\ddot{\psi}$ from the second.

One implication of this solution is that for locomotion with constant forward velocity ($\ddot{r} = 0$), a trivial solution is that $\phi = 0$, regardless of the path curvature. Any change in orientation will be effected by the skidding velocity component, which in turn comes solely from the rotor input. Consider again the serpenoid trajectory with $c(t) = \cos(t)$ and constant forward velocity $\dot{r} = 1$. The snakeboard is able to perfectly execute this gait without rotating its wheels;

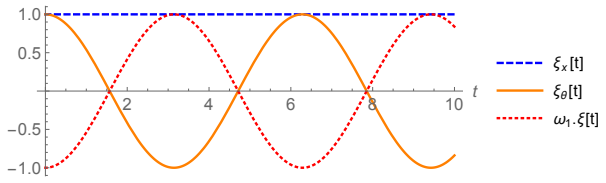

Fig. 9: Body velocities while executing the serpenoid curve with locked wheels. All turning is effected by skidding.

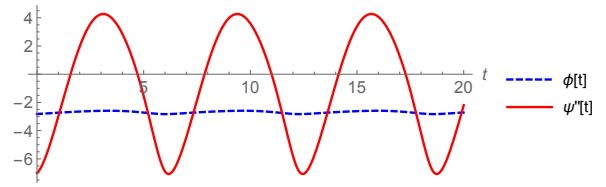

Fig. 10: Shape inputs for a trajectory with varying speed over terrain with skidding constant $k_s = 10$.

Fig. 9 shows the corresponding body and skidding velocities over time. This kind of locomotion would be impossible with the hard constraints in place, since rotor actuation has no effect when the wheels are locked at $\phi = 0$.

However, if we desire acceleration such that $\ddot{r} \neq 0$, then the space of valid exact solutions for this controller is actually quite restricted. In particular, the first line of (20) will yield a solution for ϕ only if the ratio $|\ddot{r}/\dot{r}|$ is bounded by a threshold dependent on the system parameters and path curvature. This also implies that the snakeboard cannot start from rest while exactly following a given path.

To illustrate this point, we simulate and solve for the shape inputs to execute the following trajectory: $\dot{r}(t) = 4 + \sin(t)$, $c(t) = 0.5$. This commands the snakeboard to locomote around a circle of constant curvature but with oscillating speed; here, we used a skidding coefficient of $k_s = 10$. The solved shape inputs are shown in Fig. 10. This trajectory is only possible since the system starts off with nonzero speed. If the system loses forward velocity ($\dot{r}$ decreases), navigates a wider turn ($c(t)$ decreases), or experiences greater skidding (k_s decreases), then an exact solution may not exist.

V. Conclusions and Future Work

We have shown an extension of earlier results in [10] by continuing to exploit the simple relationship between a body velocity representation for the locomoting system and a curvature parameterization for the trajectory. This has allowed us to derive exact motion planning controllers for a variety of trajectories when either viscous damping or skidding is experienced. In doing so, we took an earlier damping model and used it to guide the development of a skidding model, both using a reduced geometric formulation.

In future work we envision generalizing the results in this paper to a more general class of underactuated systems. We would also like to be able to compare our skidding model to some derived previously, namely those in [14] and [16]. It would also be instructive to explore the underlying geometry of the reduced skidding equations; for example, with some minor modification we should be able to transform the system in (19) into that of (5) and (7) in the limit of high k_s. Finally, we would like to come up with controllers, likely nonexact, for trajectories problematic for the exact ones derived in this paper, as well as scenarios with both damping and skidding simultaneously present.

References

[1] J. Ostrowski, J. Burdick, A. Lewis, and R. Murray, "The mechanics of undulatory locomotion: the mixed kinematic and dynamic case," in *Robotics and Automation, 1995. Proceedings., 1995 IEEE International Conference on*, vol. 2, may 1995, pp. 1945 –1951 vol.2.

[2] E. A. Shammas, H. Choset, and A. A. Rizzi, "Towards a unified approach to motion planning for dynamic underactuated mechanical systems with non-holonomic constraints," *The International Journal of Robotics Research*, vol. 26, no. 10, pp. 1075–1124, 2007. [Online]. Available: http://ijr.sagepub.com/content/26/10/1075.abstract

[3] J. Ostrowski, A. Lewis, R. Murray, and J. Burdick, "Nonholonomic mechanics and locomotion: the snakeboard example," in *Robotics and Automation, 1994. Proceedings., 1994 IEEE International Conference on*, may 1994, pp. 2391–2397 vol.3.

[4] R. Murray and S. S. Sastry, "Nonholonomic motion planning: Steering using sinusoids," *IEEE Transactions on Automatic Control*, vol. 38, pp. 700–716, 1993.

[5] J. Ostrowski, J. Desai, and V. Kumar, "Optimal gait selection for nonholonomic locomotion systems," in *Robotics and Automation, 1997. Proceedings., 1997 IEEE International Conference on*, vol. 1, apr 1997, pp. 786–791 vol.1.

[6] F. Bullo and A. Lewis, "Kinematic controllability and motion planning for the snakeboard," *Robotics and Automation, IEEE Transactions on*, vol. 19, no. 3, pp. 494–498, June 2003.

[7] F. Bullo and K. M. Lynch, "Kinematic controllability for decoupled trajectory planning in underactuated mechanical systems," *IEEE Transactions on Robotics and Automation*, vol. 17, pp. 402–412, 2001.

[8] E. Shammas and M. de Oliveira, "An analytic motion planning solution for the snakeboard," in *Proceedings of Robotics: Science and Systems*, Los Angeles, CA, USA, June 2011.

[9] ——, "Motion planning for the snakeboard," *The International Journal of Robotics Research*, vol. 31, no. 7, pp. 872–885, 2012. [Online]. Available: http://ijr.sagepub.com/content/31/7/872.abstract

[10] T. Dear, R. L. Hatton, M. Travers, and H. Choset, "Snakeboard motion planning with local trajectory information," in *ASME 2013 Dynamic Systems and Control Conference*. American Society of Mechanical Engineers, 2013, pp. V002T33A002–V002T33A002.

[11] S. D. Kelly and R. M. Murray, "The geometry and control of dissipative systems," in *Decision and Control, 1996., Proceedings of the 35th IEEE Conference on*, vol. 1. IEEE, 1996, pp. 981–986.

[12] A. M. Bloch, P. S. Krishnaprasad, J. E. Marsden, and R. M. Murray, "Nonholonomic mechanical systems with symmetry," *ARCH. RATIONAL MECH. ANAL*, vol. 136, pp. 21–99, 1996.

[13] J. Ostrowski, "Reduced equations for nonholonomic mechanical systems with dissipative forces," *Reports on Mathematical Physics*, vol. 42, no. 1, pp. 185–209, 1998.

[14] N. Sidek and N. Sarkar, "Dynamic modeling and control of nonholonomic mobile robot with lateral slip," in *Systems, 2008. ICONS 08. Third International Conference on*. IEEE, 2008, pp. 35–40.

[15] S. Bazzi, E. Shammas, and D. Asmar, "Novel modeling of skidding effects on the nonholonomic motion of a vertical rolling disk," in *Advanced Robotics (ICAR), 2013 16th International Conference on*. IEEE, 2013, pp. 1–6.

[16] ——, "A novel method for modeling skidding for systems with nonholonomic constraints," *Nonlinear Dynamics*, vol. 76, no. 2, pp. 1517–1528, 2014.

[17] M. P. Do Carmo and M. P. Do Carmo, *Differential geometry of curves and surfaces*. Prentice-hall Englewood Cliffs, 1976, vol. 2.

[18] A. Kelly, *Mobile Robotics: Mathematics, Models, and Methods*. Cambridge University Press, 2013.

[19] S. Hirose, "Biologically inspired robot," *Oxford University Press*, 1993.

[20] S. D. Kelly, P. Pujari, and H. Xiong, "Geometric mechanics, dynamics, and control of fishlike swimming in a planar ideal fluid," in *Natural Locomotion in Fluids and on Surfaces*. Springer, 2012, pp. 101–116.